THE ASTROPHYSICAL JOURNAL, 404:81–93, 1993 February 10

DARK MATTER AND DYNAMICS IN THE HERCULES CLUSTER (A2151)

CHRISTINA M. BIRD[1] AND JOHN M. DICKEY
Department of Astronomy, University of Minnesota, 116 Church Street, S.E., Minneapolis, MN 55455
AND
E. E. SALPETER
Cornell University, Center for Radiophysics and Space Research, Ithaca, NY 14853
Received 1992 June 15; accepted 1992 August 17

ABSTRACT

We present new 21 cm observations of faint ($15.7 < m_{pg} < 16.5$) spiral galaxies in the Hercules cluster (A2151). These results, when combined with the large body of velocities available in the literature for Hercules, permit us to study the dynamics throughout the cluster core, out to a projected radius of 1.8 h^{-1} Mpc.

We calculate the global dynamical mass of Hercules using two different, but related, methods: the virial theorem and the projected mass estimator. These masses lie in the range 3–9 $\times 10^{14}$ $M_\odot$.

We investigate the importance of subclustering in A2151 by eye, by using the statistical test of Dressler & Shectman, and by considering the effects of the detected substructure on the dynamical mass determination. The clumpy distribution of galaxies is interpreted as a sign that the galaxies in the cluster have not reached dynamical equilibrium in the gravitational potential, which means that dynamical mass estimates are subject to significant systematic errors.

Finally, we use the 21 cm line widths to estimate that the minimum total mass which is contained within the H I radii of the cluster galaxies is about 3×10^{14} h^{-1} $M_\odot$. This number is compared with the dynamical mass estimate for the entire cluster; we can then separate the contribution of dark matter inside and outside the H I envelopes of galaxies. The fraction of dark matter which cannot be associated with individual galaxies within their H I radius is about 90%–95%.

Subject headings: dark matter — galaxies: clustering — radio lines: ISM

1. INTRODUCTION

Galaxy clusters are the largest known gravitationally bound structures and, unlike the larger superclusters in which they are embedded, are at least somewhat relaxed. The dynamics of rich Abell clusters have been studied by Kent & Gunn (1982) and Beers et al. (1991), among many others, and the dynamics of the less rich Virgo Cluster by Hoffman & Salpeter (1982) and Tully & Shaya (1984). If a cluster were fully relaxed and isolated, with dark matter and galaxies distributed in the same way, the virial theorem would furnish the total gravitational mass fairly unambiguously. In that case the projected mass estimator, suggested by Bahcall & Tremaine (1981) and Heisler, Tremaine, & Bahcall (1985, hereafter HTB) to be a more statistically robust measure of mass for a dynamically evolved system, would furnish similar estimates for the total mass. In reality we have to contend with two complications, even if all matter were distributed spherically symmetrically about the cluster center: (1) the dividing surface between the bound cluster and the surrounding unbound supercluster is not well defined, so the cluster mass is not uniquely determined; (2) as pointed out by Hoffman & Salpeter (1982), the ratio of dark matter mass M to visible galaxy luminosity L may vary from the core to the outer regions of the cluster itself (quite apart from what M/L might be in the supercluster surroundings).

In clusters of galaxies, deviations from spherical symmetry may be a sign of incomplete relaxation (Beers et al. 1991; Richstone, Loeb, & Turner 1992; see also West 1990 for an opposing view). Cluster substructure is discussed by Geller & Beers (1982), Merritt (1985), Fitchett (1988), and Beers et al. (1991). Subclustering has been found even in quite rich clusters (Dressler & Shectman 1988a, b; West & Bothun 1990) and is particularly severe in an unrelaxed, spiral-dominated cluster like Virgo (see Tully & Shaya 1984 and Fig. 4 in Hoffman et al. 1989). A study of the classical Hercules Cluster A2151 is particularly interesting in this regard because (1) it is intermediate in richness between the Virgo Cluster and the well-studied Coma Cluster, A1656; and (2) the surrounding supercluster is elongated and has two other prominent clusters within it (A2147 and A2152). A2151 is very well observed, so many velocities for its galaxies exist in the literature (Tarenghi et al. 1979; Giovanelli & Haynes 1985; Salpeter & Dickey 1985; Dressler & Shectman 1988a; Huchra 1990). We have obtained 12 new observations of faint spirals at Arecibo[2] to supplement this sample. We use the combined sample to study the substructure in the cluster and to discuss the cluster mass and its uncertainties.

Rotation curves for resolved spiral galaxies provide evidence for dark matter within the galaxies themselves (Faber & Gallagher 1979; Begeman 1987; Puche 1991), even when the rotation curve shows a decline (Casertano & van Gorkam 1991). Twenty-one cm H I data is particularly useful as a probe of the halo mass distribution, since the neutral hydrogen disk typically extends about a factor of 1.5 further out than the optical disk, measured at R_{25} (Warmels 1986). Most galaxies in A2151 are unresolved by the Arecibo beam at 21 cm, but the velocity width of the H I line gives the maximum rotation velocity. Coupled with the radius of the galaxy, this gives the "indicative mass" of each measured galaxy, that is, the total gravitating mass (comprised by stars, gas, and dust, as well as

[1] Postal address: Department of Physics and Astronomy, Michigan State University, East Lansing, MI 48824.

[2] The Arecibo Observatory is part of the National Astronomy and Ionosphere Center, which is operated by Cornell University under a cooperative agreement with the National Science Foundation.

dark matter), but only out to the edge of the disk. After applying a correction for the galaxies in the cluster not observed in H I, we shall obtain the "summed indicative mass" of the cluster galaxies to compare with the virial theorem mass estimate.

In § 2 we discuss the new Arecibo observations. Section 3 summarizes the velocity information available in the literature, as well as the selection criteria for the final data set. Section 4 contains a discussion of the structure of A2151 and its relation to the surrounding Hercules Supercluster. In § 5 we discuss the variety of dynamical mass estimators, in § 6 the indicative galaxy masses and their relationship to the cluster dynamical mass. Finally, in § 7 we present a summary and discussion of the structure and dynamics in A2151.

2. NEW OBSERVATIONS

Candidate galaxies for the survey were selected from the catalog of galaxies in Hercules generated by the Minnesota Automated Plate Scanner (Dickey et al. 1987). The APS list contains positions, magnitudes, and colors (with rms errors of 0.25 and 0.20 mag, respectively) for galaxies down to limiting magnitude $m_J = 18.5$. Dickey et al. estimate the APS catalog to be 80% complete or better at this magnitude.

The distribution of morphological type in color is fairly well determined for types later than Sb. Dickey et al. estimate that for $J-F < 0.8$ ("blue"), only 15% of that subset as selected by the APS are elliptical, S0, or Sa galaxies. Choosing galaxies with $J-F < 0.9$ provides a list of candidate H I objects which suffers from roughly 25% contamination by early morphological types. It should, however, include 85% of all late-type spirals in the cluster. This provides us with a complete list of optically selected spiral galaxies for a radio survey.

We obtained H I observations for the 22 brightest (in m_{ph}) previously unstudied galaxies in 1988 February, using the 305 m Arecibo telescope and the 22 cm circular feed. The circular feed is remotely "tunable," which allows one to maximize gain and minimize sidelobe response for frequencies other than the nominal center frequency of the feed. This optimizes the sensitivity of the telescope, allowing higher detection rates for galaxies which are at velocities similar to that of Hercules [v(H I| 11,050 km s^{-1}) = 1370 MHz]. The circular feed also allows observations of both circular polarizations simultaneously, effectively halving the required integration time for each observation for equal S/N.

The spectra were measured by the 1048 channel autocorrelator, which has a Nyquist frequency of 40 MHz. Each independent polarization was split in two by feeding 10 MHz slices of the total bandwidth into separate quadrants of the autocorrelator, yielding four 512 channel spectra with 39.1 kHz channel spacing. Since optical redshifts were unavailable for the candidate galaxies, the "search moded" of the autocorrelator was used. This consists of overlapping the quadrant edges by 7.5 MHz, which allows a total bandwidth of 32.5 MHz, that is, velocity coverage of about 7300 km s^{-1}.

Observations were made in total power mode, with five minutes of integration on the source followed by five minutes on blank sky. Each undetected source was observed for a total of 15 minutes before a new velocity range was chosen to continue the search. The final spectrum produced for each galaxy was the weighted, accumulated average of all ON-OFF pairs. One of the primary limitations in using the Arecibo telescope at such high recessional velocities is the strong interference at these frequencies. This interference is caused primarily by the FAA radar at the airport in San Juan, but also by equipment at the observatory site. A useful clean detection can only be made if a galaxy's peak happens to fall between the interface spikes. Toward the end of the observing run, J. Dickey and M. Davis designed and implemented a prototype radar blocker which has since been put into use to help prevent contamination of spectra by the FAA radar.

The observations were reduced using the ANALYZ and GALPAC data analysis packages, supplied by the Arecibo computing staff and installed on a Sun Sparcstation at the University of Minnesota. Spectra were weighted by gain and system temperature corrections for each observation, since both of these are affected by the zenith angle of the source. Gain is substantially degraded as a source moves away from zenith; system temperature is sensitive to zenith angle because the feed illustration pattern sees the ground instead of the telescope reflector for zenith angles greater than 10°. The spectra were also weighted by a value based on the frequency response of the feed (see Haynes & Giovanelli 1984 for a full discussion of these effects.) The spectra were smoothed using a 3 channel boxcar, followed by Hanning smoothing, and the observed quantities were measured from the resultant spectra after subtraction of the baseline. Calibration of absolute flux levels was achieved by comparison of the measured fluxes of the bright compact sources 3C 48, 0138+13, 0947+14, 0202+14, and −127+23 to the flux measurements in the Bridle et al. (1972) bright source catalog.

Final measured parameters for the 12 new H I detections are given in Table 1. Galaxy velocities (col. [4]) typically have

TABLE 1

NEW OBSERVATIONS

Designator	R.A.	Declination	Velocity (km s^{-1})	Integral (mJy km^{-1} s^{-1})	Line Width (km s^{-1})
H27	16^{h}04^{m}33^s.3	17°37′34″	11199	984	221
H44	16 05 09.3	17 47 40	11546	1390	444
H47	16 03 14.7	17 48 55	11086	1674	325
H60	16 03 11.4	17 26 31	11084	2395	331
H78	16 03 21.5	17 56 08	10266	4670	600
H84	16 01 01.4	17 56 00	11268	428	128
H87	16 04 42.3	17 59 23	11517	1175	252
H129	16 02 44.1	18 19 20	11355	499	329
H138	16 05 39.9	18 25 41	10810	1209	306
H147	16 04 03.3	18 29 43	10958	795	413
H154	16 00 35.4	18 34 58	12252	1136	374
H1559174	15 59 34.4	17 46 45	10736	1609	141

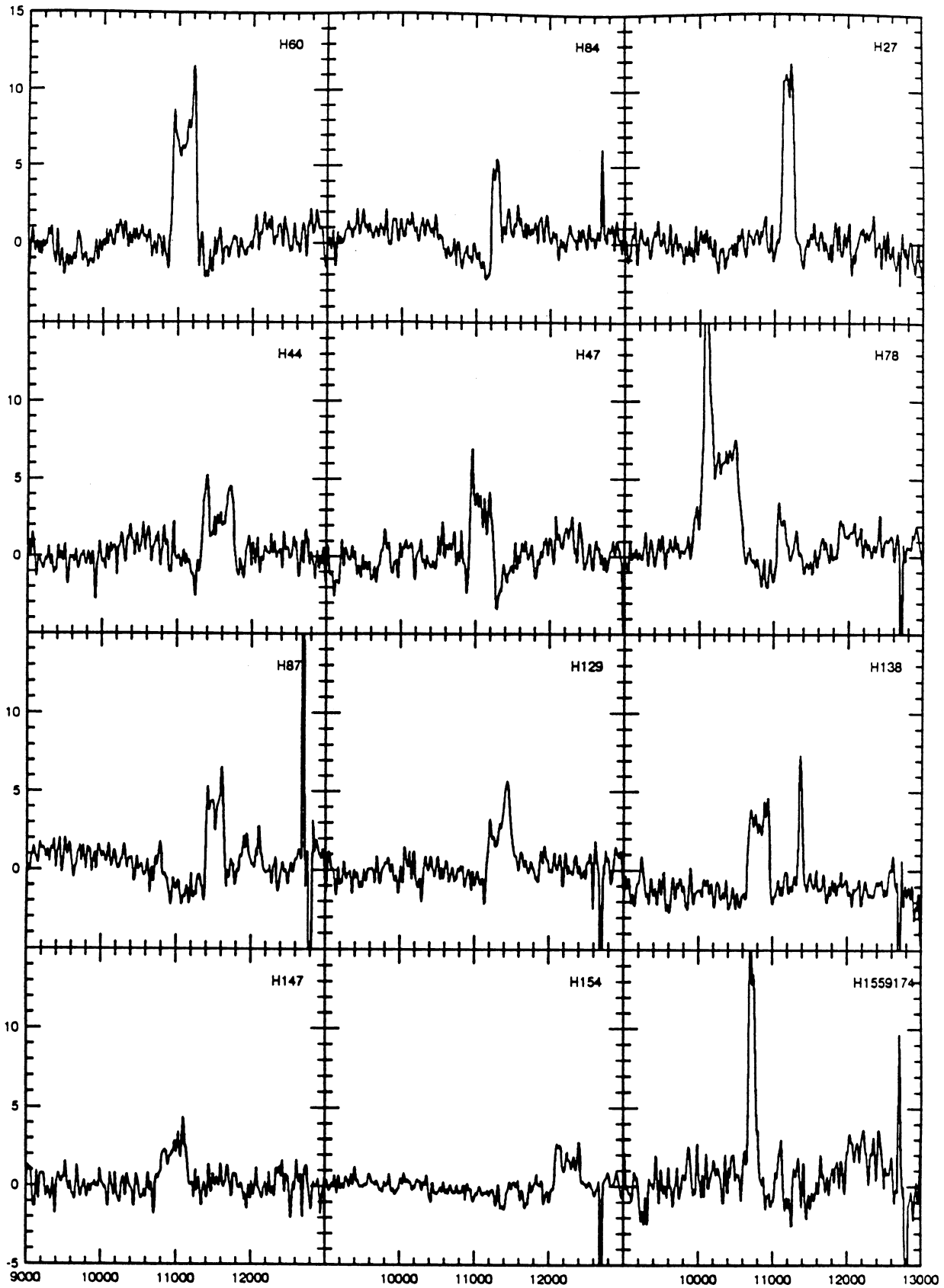

FIG. 1.—New Arecibo 21 cm observations. The horizontal axis is in km s^{-1}; the vertical axis is flux in mJy. The galaxy designator, corresponding to col. (1) of Table 1, is given in the upper right corner of each spectrum.

errors of 8 km s^{-1}. The line widths given in column (6) are measured at the 20% of the peak of the feature (after baseline subtraction) and are reliable at the 90% confidence level (Bicay & Giovanelli 1986). The spectra themselves are presented in Figure 1.

3. PREVIOUSLY OBTAINED DATA AND OUR FINAL GALAXY LIST

A large number of radial velocities for galaxies in A2151 have been measured by other observers. Tarenghi et al. (1979) observed the area of the Hercules Supercluster and measured optical redshifts for more than 170 galaxies and components in A2151 and the surrounding area (a total of 28 deg^2). Dressler & Shectman (1988a) obtained 102 galaxy redshifts in Hercules as part of their study of substructure in rich clusters. Giovanelli & Haynes (1985) observed 14 Hercules galaxies in H I, detecting 10; and Salpeter & Dickey (1985) mapped the cluster in H I using the D-configuration of the VLA, finding 31 galaxies. The CfA survey (Huchra 1990) contains 93 galaxies in the area of A2151 for which optical measurements have been made. We compared these lists to eliminate any duplications, choosing H I redshifts preferentially and optical redshifts with quoted errors when available, and combined them with our new observations to form the data set below. The surrounding supercluster has been studied by Freudling (1990) and by Freudling, Haynes, & Giovanelli (1992). Fortunately supercluster contamination of A2151 is small. We adopt the cluster center (R.A. = $16^h03^m11^s$, decl. = 17°55′55″) and core radius $R_c = 28'$ from Tarenghi et al. (1979) and consider as potential members of A2151 all galaxies within $2R_c = 3360'' = 0.^\circ9$ of the cluster center. We accept for inclusion in our galaxy list the wider velocity range of 9000–14,000 km s^{-1} and discuss membership and the significance of outliers below.

Our selection criteria give us a data set of 127 galaxies, which are listed in Table 2. Column (1) lists the position within our data set, which is given in order of increasing declination; column (2) lists the NGC, IC, or Zwicky catalog number, if available; columns (3) and (4) list the right ascension and declination (1950.0); columns (5) and (6) list the x' and y' offsets with respect to a coordinate axis rotated through the 20° position angle of the cluster (see the next section for a discussion of its elongation); column (7) lists the heliocentric velocity; column (8) lists the separation of the galaxy from the fiducial cluster center; column (9) lists the photographic magnitude from the APS catalog; and column (10) gives the $J-F$ color, also from the APS.

The average velocity for the complete data set is 11,059 km s^{-1}; the velocity dispersion is 726 km s^{-1}. The individual velocities are displayed in Figure 2 (as a function of the separation R from the cluster center). The velocity distribution is shown in Figure 3. On the high-velocity side there are three suspicious galaxies, numbers 12, 25, and 113, with velocities of 12,873, 13,451, and 13,682 km s^{-1}, respectively, which are located in the extreme upper tail of the distribution. These may adversely affect the statistical estimates for the cluster.

The number distribution $N_{gal}(R) = 2\pi R n(R)$, the projected surface density at projected radial distance R, is plotted against R in Figure 4 to assist in the separation between cluster members and supercluster contamination. Note that the distribution is fairly flat ($n \propto R^{-1}$) for $R < R_c \approx 1600''$. Tarenghi et al. determined the nominal cluster center by taking the luminosity-weighted average of their data set. Beers & Tonry (1986) argue that the constant number density of galaxies within R_c is a signal that luminosity weighting is not locating the physically meaningful centroid. There is no dominant galaxy in A2151 which might be located at the dynamical center of the cluster, and the X-ray structure is complex, so choosing an independently determined centroid is not straightforward. In any event, outside R_c, the shape of the number density is much less sensitive to the choice of center. The falloff beyond 1600″ is almost $n \propto R^{-2}$ (steeper than the Virgo Cluster), so the density contrast between the cluster and supercluster is distinct, at least insofar as the light distribution is concerned (see also § 5). Figure 5 gives a contour map of the projected number density of galaxies (see § 4 for a more complete discussion of the adaptive kernel method).

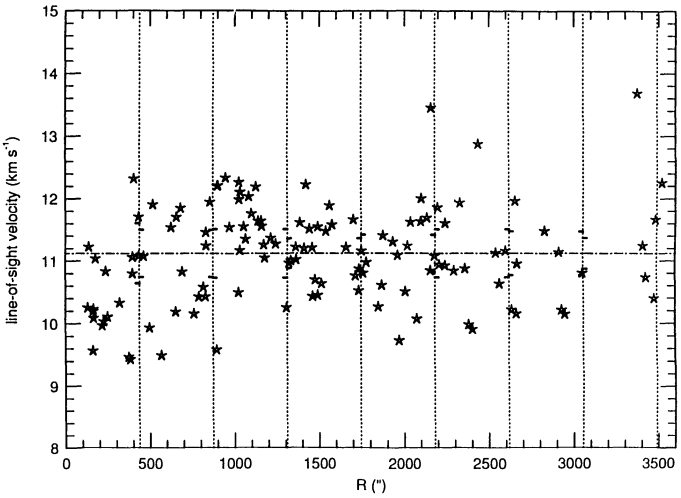

FIG. 2.—All galaxies with published redshifts, plus new Arecibo observations, within 2 core radii of the cluster center and with velocities between 9000 and 14,000 km s^{-1}.

We have determined the centroid, average velocity, and velocity dispersion separately for four classes of galaxies, divided into "faint" and "bright" ($m_{ph} = 16.0$ for the cutoff magnitude) and "red" and "blue" (with $J-F < 0.9$ defining blue). There were no obvious trends in the distributions of

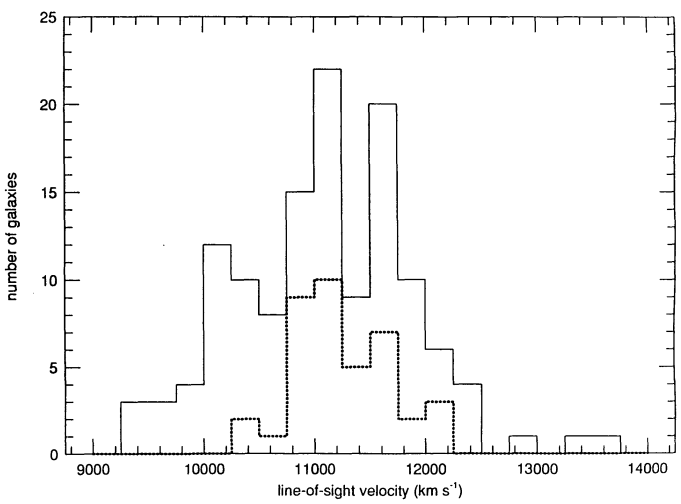

FIG. 3.—Velocity histogram of A2151. The smaller histogram, bordered by the heavy dotted line, is the velocity histogram for the clump identified by the Dressler-Shectman test.

TABLE 2

THE COMPLETE DATA SET

BDS Number	Other Name	R.A.	Declination	X'	Y'	Velocity (km s^{-1})	R	m_{ph}	$J-F$	Source
1.....	...	16^{h}01^{m}06^s.5	17°11′43″	−762″	−3100″	11666	3192″	16.0	0.00	DS88
2.....	...	16 00 33.4	17 18 20	−1341	−2888	10399	3184	14.0	0.00	DS88
3.....	...	16 02 03.9	17 19 00	−142	−2409	10217	2413	15.0	100.00	DS88
4.....	...	16 01 23.3	17 19 17	−692	−2591	10217	2682	16.0	0.00	DS88
5.....	108–151	16 04 27.5	17 19 40	1770	11962	−1671	2434	15.3	0.00	GH85
6.....	N6034	16 01 16.0	17 20 12	−809	−2575	10150	2699	15.2	0.00	DS88
7.....	108–088	16 01 32.6	17 22 36	−635	−2359	10953	2443	15.3	0.00	GH85
8.....	...	16 01 47.1	17 25 06	−492	−2147	9908	2203	14.0	0.00	DS88
9.....	...	16 03 30.9	17 26 23	873	−1568	11088	1795	17.5	0.48	Z-cat
10.....	...	16 01 41.1	17 26 29	−601	−2098	9982	2183	16.5	1.19	DS88
11.....	...	16 03 37.7	17 26 31	961	−1527	9728	1805	17.0	0.98	DS88
12.....	...	16 01 25.0	17 28 28	−858	−2065	12873	2235	16.4	0.16	Z-cat
13.....	...	16 03 38.5	17 28 29	932	−1413	10266	1692	16.7	0.48	SD85
14.....	...	16 02 32.1	17 28 58	32	−1709	10610	1710	16.3	0.49	SD85
15.....	108–133	16 03 29.0	17 29 48	777	−1385	10522	1588	14.8	1.13	GH85
16.....	...	16 00 58.5	17 30 15	−1250	−2094	10155	2438	16.0	1.08	DS88
17.....	...	16 02 57.0	17 33 25	274	−1337	10452	1365	15.2	0.83	SD85
18.....	...	16 01 12.4	17 34 11	−1144	−1804	11932	2136	16.0	1.19	DS88
19.....	...	16 02 04.0	17 34 19	−455	−1545	10804	1610	16.4	0.80	SD85
20.....	108–108	16 02 30.2	17 34 58	−117	−1380	10638	1385	15.8	0.00	SSB81
21.....	...	16 03 52.0	17 35 38	966	−944	10699	1350	15.3	1.09	DS88
22.....	108–098	16 02 14.6	17 36 13	−352	−1386	11889	1430	15.8	0.47	GH85
23.....	...	16 04 33.3	17 36 26	1503	−697	11199	1601	15.7	0.52	BDS93
24.....	...	16 03 34.8	17 36 49	711	−961	10255	1195	16.9	1.05	DS88
25.....	...	16 01 17.1	17 36 59	−1138	−1623	13451	1981	15.9	0.65	Z-cat
26.....	...	16 03 30.2	17 40 28	172	−924	12263	940	16.1	0.73	SD85
27.....	...	16 03 30.3	17 42 59	524	−635	12206	823	17.5	0.48	SD85
28.....	...	16 01 52.1	17 43 04	−794	−1110	11548	1364	16.7	1.06	DS88
29.....	...	16 04 26.0	17 43 31	1260	−333	12226	1302	17.3	0.09	Z-cat
30.....	I1178	16 03 18.7	17 44 01	348	−633	10425	722	14.3	1.13	DS88
31.....	I1181	16 03 17.9	17 44 25	329	−615	10154	697	15.3	100.00	DS88
32.....	...	15 59 34.4	17 46 45	−2715	−1574	10737	3139	16.1	0.23	BDS93
33.....	...	16 02 34.0	17 46 46	−308	−696	11462	761	17.0	1.07	Z-cat
34.....	...	16 04 33.2	17 46 53	1287	−108	11201	1291	16.2	0.79	Z-cat
35.....	...	16 02 52.0	17 47 02	−72	−594	10186	598	16.8	0.77	SD85
36.....	...	16 02 13.7	17 47 03	−586	−780	11354	975	16.6	1.17	Z-cat
37.....	...	16 03 03.6	17 47 25	75	−515	9493	521	17.3	0.95	DS88
38.....	...	16 05 09.3	17 47 40	1755	112	11479	1759	15.8	0.89	BDS93
39.....	...	16 03 14.7	17 48 55	194	−377	11077	423	15.9	1.06	BDS93
40.....	...	16 03 41.3	17 49 40	535	−205	11540	572	16.9	0.94	DS88
41.....	...	16 05 02.1	17 49 44	1616	194	10977	1627	16.5	1.09	Z-cat
42.....	...	16 03 11.4	17 49 52	130	−339	11062	363	16.5	0.56	BDS93
43.....	...	16 04 12.0	17 50 00	939	−36	11987	940	16.6	1.05	Z-cat
44.....	N6042	16 02 24.0	17 50 00	−509	−563	10430	758	14.8	1.24	TT79
45.....	...	16 03 48.1	17 50 08	616	−145	10829	633	17.0	0.98	DS88
46.....	...	16 02 24.6	17 50 10	−504	−551	10581	746	14.8	1.24	DS88
47.....	...	16 03 00.8	17 50 35	−27	−351	9432	352	16.5	0.99	DS88
48.....	I1193	16 04 17.2	17 50 51	992	37	12034	992	15.3	1.19	DS88
49.....	108–134	16 03 30.0	17 51 06	354	−179	11078	396	15.1	0.94	GH85
50.....	N6041	16 02 21.0	17 51 24	−577	−499	11248	763	14.2	1.09	DS88
51.....	I1170	16 02 16.8	17 51 25	−634	−518	9587	819	15.8	1.13	DS88
52.....	N6047	16 02 53.8	17 51 55	−149	−310	9470	343	14.5	1.21	DS88
53.....	...	16 01 03.2	17 52 10	−1636	−835	10507	1837	16.5	0.94	DS88
54.....	N6040	16 02 11.3	17 52 39	−733	−476	12336	868	15.2	0.00	Z-cat
55.....	I1179	16 03 07.6	17 53 20	8	−162	11040	162	15.6	0.84	SD85
56.....	N6050	16 03 08.5	17 53 31	16	−148	9571	148	15.2	0.84	SD85
57.....	N6045	16 02 53.1	17 53 31	−191	−223	10330	293	14.7	0.85	SD85
58.....	...	16 04 24.5	17 53 39	1032	231	11642	1057	15.4	1.13	DS88
59.....	I1183	16 03 23.4	17 54 07	203	−41	10038	207	15.2	1.18	DS88
60.....	N6054	16 03 15.9	17 54 10	102	−75	11225	126	15.9	0.48	SD85
61.....	...	16 03 19.1	17 54 17	142	−53	10233	152	17.3	0.74	DS88
62.....	N6043	16 02 45.7	17 54 32	−311	−201	12320	370	15.3	1.06	TT79
63.....	I1172	16 04 18.3	17 54 34	930	252	11547	964	15.5	0.99	DS88
64.....	I1194	16 04 24.0	17 55 00	984	342	11642	1042	15.5	1.03	TT79
65.....	...	16 04 05.9	17 55 17	749	232	11950	784	16.9	0.94	DS88
66.....	...	16 04 21.5	17 55 45	949	335	11760	1106	16.8	1.29	DS88
67.....	...	16 01 01.4	17 56 00	−1753	−590	11240	1849	16.0	0.61	BDS93
68.....	...	16 03 27.0	17 56 03	212	86	10110	228	18.4	−0.35	SD85
69.....	...	16 03 25.0	17 56 06	184	79	9973	200	18.3	0.15	Z-cat
70.....	I1182	16 03 21.5	17 56 08	137	64	10266	150	14.5	1.09	BDS93

TABLE 2—*Continued*

BDS Number	Other Name	R.A.	Declination	X'	Y'	Velocity (km s^{-1})	R	m_{ph}	$J-F$	Source
71*.....	...	16^{h}03^{m}12^s.8	17°57′53″	−16″	120″	10254	121″	16.3	0.88	DS88
72.....	...	16 02 47.0	17 57 57	−363	−2	10797	364	16.5	0.97	DS88
73.....	...	16 04 51.3	17 58 55	1283	659	11582	1441	16.0	1.07	Z-cat
74*.....	...	16 03 07.8	17 59 22	−114	179	10834	217	16.0	1.29	DS88
75.....	...	16 04 42.3	17 59 23	1153	641	11517	1319	16.7	0.52	BDS93
76.....	...	16 04 51.3	18 00 13	1256	732	11582	1443	16.0	1.07	DS88
77.....	N6044	16 02 44.9	18 00 19	−440	121	9936	456	15.2	0.99	DS88
78.....	...	16 02 08.1	18 00 50	−944	−30	11170	945	16.0	1.20	DS88
79.....	108–149	16 04 20.8	18 01 30	821	655	11049	1078	15.7	0.91	GH85
80.....	N6056	16 03 12.0	18 02 30	−120	377	11707	395	15.5	100	TT79
81.....	...	16 04 18.5	18 03 20	753	748	11558	1060	15.8	0.90	DS88
82.....	...	16 04 07.8	18 03 45	601	719	10494	937	16.4	1.00	DS88
83.....	...	16 03 14.6	18 03 47	−113	461	11906	475	16.2	1.16	DS88
84*.....	...	16 03 59.2	18 05 17	454	763	11540	888	16.2	0.35	SD85
85.....	I1176	16 03 16.7	18 05 51	−127	588	11707	602	14.8	1.16	DS88
86.....	...	16 03 07.3	18 06 18	−263	567	11851	625	16.9	0.90	DS88
87.....	...	16 01 55.4	18 07 02	−1241	258	11616	1268	16.4	1.13	DS88
88*.....	108–135	16 03 30.8	18 08 52	0	827	12212	827	15.6	1.00	SSB81
89.....	...	16 02 25.4	18 09 08	−882	523	11259	1073	16.7	0.97	DS88
90.....	...	16 04 47.1	18 09 19	1013	1225	10870	1589	15.7	0.87	DS88
91.....	...	16 03 51.0	18 10 12	243	1001	12190	1030	16.2	0.80	SD85
92*.....	...	16 05 17.0	18 10 24	1392	1431	11078	1997	16.0	1.02	DS88
93.....	108–129	16 03 25.4	18 11 18	−122	938	12106	946	15.5	1.03	SSB81
94*.....	...	16 03 59.2	18 12 42	302	1182	11002	1219	17.0	1.08	DS88
95.....	...	16 03 45.9	18 12 57	118	1131	11273	1137	16.5	1.10	DS88
96*.....	...	16 03 26.4	18 14 23	−172	1116	11368	1151	16.3	1.21	DS88
97*.....	108–138	16 03 47.8	18 14 47	106	1243	11022	1248	16.0	0.48	GH85
98*.....	...	16 03 34.6	18 15 16	−81	1206	10967	1209	17.1	0.77	DS88
99*.....	...	16 03 10.4	18 16 41	−434	1168	11220	1246	18.1	0.49	Z-cat
100*.....	...	16 03 51.4	18 17 20	102	1405	11479	1408	18.0	0.00	SD85
101.....	N6055	16 03 18.4	18 17 34	−345	1257	11212	1334	14.8	1.30	DS88
102*.....	N6057	16 03 25.4	18 17 56	−259	1312	10433	1337	15.5	1.27	DS88
103*.....	108–144	16 04 00.5	18 19 03	189	1546	11662	1557	15.6	0.88	GH85
104*.....	...	16 04 58.8	18 19 27	962	1853	11858	2016	15.6	0.88	DS88
105*.....	108–139	16 03 45.6	18 19 43	−25	1511	11215	1519	15.0	0.85	GH85
106*.....	...	16 03 38.4	18 21 16	−153	1563	10760	1570	15.3	0.93	SD85
107*.....	...	16 04 38.9	18 21 21	657	1863	10845	1975	16.1	1.14	DS88
108*.....	...	16 05 11.2	18 22 37	1064	2092	10634	2347	16.8	1.07	DS88
109*.....	N6061	16 04 00.0	18 23 00	88	1767	11305	1769	14.4	1.32	TT79
110.....	...	16 04 29.4	18 23 13	491	1922	11603	2053	17.8	0.32	SD85
111*.....	...	16 04 15.7	18 24 06	289	1905	11998	1927	15.8	0.98	DS88
112*.....	...	16 04 14.8	18 24 08	276	1902	11632	1922	15.0	0.98	DS88
113.....	...	16 00 10.0	18 24 13	−3007	713	13682	3090	15.6	1.08	DS88
114*.....	108–127	16 03 21.5	18 24 23	−443	1656	11407	1715	15.5	0.63	GH85
115*.....	...	16 05 39.9	18 25 13	1395	2379	10808	2796	16.6	0.60	BDS93
116*.....	...	16 03 05.8	18 26 59	−707	1726	11622	1866	16.0	0.95	DS88
117*.....	...	16 02 09.2	18 27 43	−1481	1491	10840	2102	16.8	1.22	DS88
118*.....	...	16 03 57.6	18 27 45	−29	2022	10940	2022	16.8	1.22	SD85
119*.....	...	16 03 13.4	18 28 31	−637	1850	11690	1956	16.5	0.59	SD85
120*.....	...	16 04 03.3	18 29 43	8	2161	10876	2161	16.4	0.90	BDS93
121*.....	...	16 03 02.2	18 30 05	−819	1884	10926	2054	16.9	0.98	BDS93
122*.....	108–146	16 03 59.5	18 32 57	−110	2325	11129	2327	15.7	0.00	GH85
123.....	...	16 00 35.4	18 34 58	−2887	1443	12252	3227	16.3	0.73	BDS93
124*.....	...	16 03 37.9	18 35 45	−457	2377	11161	2380	15.7	100.00	DS88
125*.....	...	16 05 25.0	18 37 05	952	2975	11242	3124	15.7	0.88	DS88
126*.....	...	16 03 36.0	18 40 00	−583	2645	11139	2669	15.6	1.16	TT79
127*.....	108–140	16 03 48.2	18 48 10	−573	3128	11571	3239	15.6	0.87	GH85

NOTES.—Asterisk in the first column indicates a subgroup member selected by the Dressler-Shectman analysis. References for velocities: DS88 = Dressler & Shectman 1988a, b; GH85 = Giovanelli & Haynes 1985; BDS93 = this paper; Z-cat = CfA redshift survey; SD85 = Salpeter & Dickey 1985; SSB81 = Schommer et al. 1981.

these galaxies, that is, mass segregation and morphological separation is not a significant effect in A2151.

4. ELONGATION AND SUBCLUSTERING

The spatial distribution of the galaxies, along with the location of the X-ray centroids of the *Einstein* map of Magri et al. (1987), is presented in Figure 5. This map was created using the adaptive kernel software kindly provided by Timothy Beers and the APS Hercules catalog, which contains 167 galaxies brighter than $m_{ph} < 17.0$, to roughly correspond to the same magnitude range as our data set. Briefly, the adaptive kernel technique provides optical density maps for sparse (low-N) data sets. The smoothing size selected by the software depends on the local number density of galaxies. As the local density

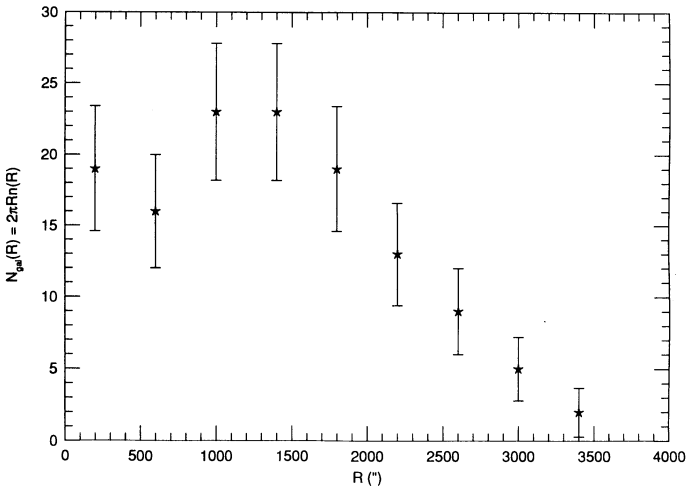

FIG. 4.—Number of galaxies, in circular annuli, vs. projected radius from the nominal cluster center (R.A. = $16^h03^m11^s$, decl. = 17°55′55″), $N_{gal}(R) = 2\pi Rn(R)$, where $n(R)$ is the projected number density.

galaxies increases, the smoothing scale decreases, so the map is sensitive to small-scale structure. At low local densities, the smoothing scale increases, thus smoothing over Poissonian fluctuations in outer regions of the cluster (see Beers et al. 1991 and references therein for a full discussion of the technique). The X-ray contour map (Fig. 1*f* of Magri et al.) shows a clear two-component structure, although the fainter, eastern lobe is too weak to be clearly distinguished from the brighter western component in their model fit. The asphericity of these two distributions is obvious.

Guided by the pronounced asymmetries in the optical and X-ray distributions, we next turn to statistical diagnostics of the three-dimensional position and radial velocity phase space to probe the structure of A2151. We have written computer algorithms to reproduce the "cumulative deviation" test of Dressler & Shectman (1988b, hereafter DS) and the "centroid shift" test of West & Bothun (1990) as alternative means to look for substructure. Bird (1992) gives a detailed account of the use of both of these tests on the data in our Table 2, and we only quote results here: the DS test yields a cumulative deviation for all galaxies in A2151 which is 12 σ above that expected for a relaxed spherical distribution; the West-Bothun test yields a 5 σ result. Both of these are highly significant (although not quite as strong as an equivalent treatment of the Virgo Cluster; see Bird 1992), that is, both of these diagnostics indicate the presence of a strong correlation between position and velocity dispersion. The DS test can also be used to attempt to identify individual subgroups, although the results depend on various parameter choices and may be somewhat ambiguous. Bird (1992) has used a variant of this approach which furnishes only one subgroup or "clump" in addition to the remaining main cluster. The clump members are denoted by an asterisk in Table 2.

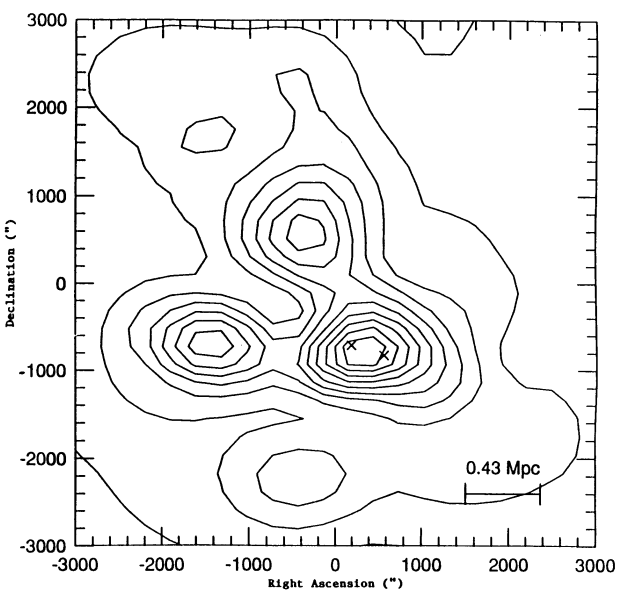

FIG. 5.—The adaptive kernel map (see Beers et al. 1991) for the APS galaxies with magnitudes above 17.0 photographic (corresponding roughly to the limiting magnitude of our data set). The contours are linearly spaced in units of 0.0257 galaxies arcmin^2 and range from 0.0015 to 0.2582 galaxies arcmin^2 from highest to lowest. The crosses indicate the centroids of the Magri et al. (1988) *Einstein* X-ray map of the cluster.

The DS-selected clump has 34 members (with 90 left in the main cluster); its center is at R.A. = $16^h03^m52^s$, decl. = 18°20′59″, with V_{av} = 11258 km s^{-1} and σ = 462 km s^{-1} (referred to the clump mean). With a few exceptions, the clump members are simply the galaxies with the largest positive y' (northwestern end), with a dividing line near $y' = 1000''$. The subregion of the velocity distribution in Figure 3 (bordered by a heavy dotted line) indicates the DS clump, showing the smaller σ_v. It is interesting to note that unlike clusters which are clearly superpositions of distinct populations in velocity, such as Cancer (Bothun et al. 1983) and Centaurus (Lucey, Currie, & Dickens 1986), identification of the dynamically distinct subgroup does not lead to a reduction in the global cluster σ_v. The central locations of the subgroup and main concentration are also similar: V_{av} = 11258 km s^{-1} for the subgroup and 10,975 km s^{-1} for the main concentration. These facts may mean that the subclump has already undergone significant interaction with the gravitational potential of the cluster, but still retains some memory of its dynamical integrity. They also indicate that the substructure, while significant as a clue to the dynamical age of A2151, is going to provide an uncertainty in dynamical mass estimates which is somewhat difficult to quantify. Based on calibration of our substructure method against the detailed dynamical mass models of the Virgo Cluster (Hoffman & Salpeter 1982; Tully & Shaya 1984), we estimate that these uncertainties are about 20%.

The adaptive kernel map in Figure 5 strongly suggests the presence of a second clump to the east of the main concentration, but there are not sufficient redshifts measured in that area for the Dressler-Shectman test to decide whether it is a kinematically distinct structure. Neglecting this unverified western clump, the remaining contours in the adaptive kernel map are elongated along a southwest-northeast axis, and it is instructive to refer galaxy positions to this axis. We therefore define two Cartesian coordinates,

$$x' = \text{R.A. cos (20°)} - \text{decl. sin (20°)}\,,$$
$$y' = \text{R.A. sin (20°)} + \text{decl. cos (20°)}\,, \quad (1)$$

so that y' is the position along the major axis and x' along the minor axis. The degree of elongation can be judged from Figure 6, where the solid line gives the distribution over bins in

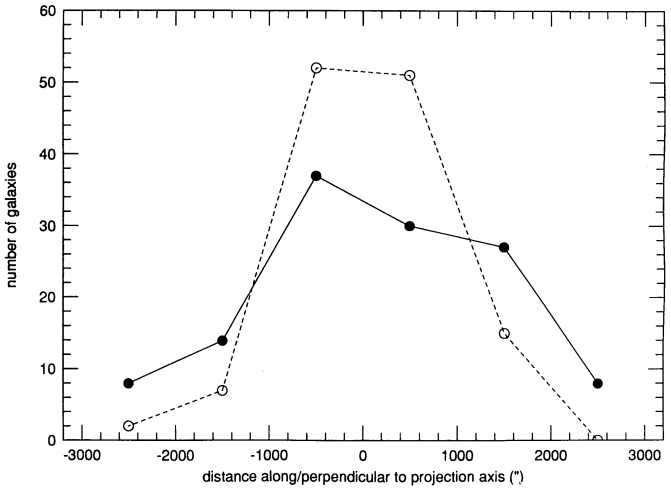

FIG. 6.—Number of galaxies in bins along the major and minor axes of the cluster. The filled circles and solid lines indicate the bins along the axis of elongation (in the y'-coordinate). The open circles and dashed lines indicate bins perpendicular to the elongation of the cluster (in x').

y' and the dotted one gives the equivalent x' distribution, which is noticeably narrower. Note also that the southward extension of the major axis, from the A2151 center, passes between A2147 and A2152.

Figure 7 shows the velocity distributions for 1000″ bins along the y'-axis. The two outer bins show a markedly peaked distribution, which may indicate that these galaxies are internally bound, that is, form dynamically distinct entities within the global cluster gravitational potential. Figure 8*a* gives the velocity profile along the y'-axis. There is evidence for a small gradient in mean velocity, or else a "clump" of low-velocity galaxies in the northeast ($y' < -2000''$). Figure 8*b* gives the velocity dispersions (about the overall cluster velocity mean). There exists a larger dispersion in the northeast, the nearer side to the two neighboring clusters. Note that this is southwest-notheast gradient, not a variation of σ with $|y|$ (the values of σ_v averaged at $y' = \pm 500''$, $\pm 1500''$, and $\pm 2500''$ are approximately constant).

In Figure 9 we present the σ_v-projected radius relation. The dip at about 1400″ is statistically significant (see Appendix), and may also be a signature of a previous merger between two similarly sized clumps. The profile is consistent with a constant value of σ_v out to our limiting radius and may indicate that supercluster contamination is more important at large distances from the cluster centroid.

To summarize the situation on substructure in A2151, we have two tentative conclusions: the cluster is not relaxed, since it clearly deviates from a spherical distribution in projection and a Gaussian velocity distribution, and the structure involves elongation in a roughly southwest-northeast direction. The *Einstein* map supports these conclusions, although the scale of the bimodality in the X-rays is rather smaller than that which we find in the galaxy distribution and velocities: about 400″–500″ separates the X-ray centroids, whereas our clump is about 1000″ from the cluster center. These results are not inconsistent, since *Einstein* is only sensitive to cluster emission on the order of 10′–12′ from the center of a bright cluster (Mushotzky 1992, private communication), and A2151 is not a bright X-ray emitter. *ROSAT* images may be more revealing of X-ray structure on a scale similar to the optical structure we have discussed above.

5. CLUSTER MASS ESTIMATES AND UNCERTAINTIES

The virial theorem, the conventional method of dynamical mass determination for a relaxed system, may be derived from the collisionless Boltzmann equation (cf. Binney & Tremaine 1987). For a steady state system, the phase space distribution of mass is constant, and under the assumptions of a spherically symmetric distribution of test particles and a known distribution of gravitating mass, the virial theorem uniquely specifies the total mass. In the present situation, we have assumed that the luminous particles trace the shape of the gravitational potential, although there is some evidence (Briel et al. 1991; Buote & Canizares 1992; Tyson 1992) that in fact the dark matter in clusters is more concentrated than the galaxies. In the absence of any more detailed knowledge about the distribution of galaxy orbits in A2151, we will assume that they are isotropic, so that $\sigma_{x\,\mathrm{transverse}} = \sigma_{y\,\mathrm{transverse}} = \sigma_{\mathrm{radial}}$.

We have 127 galaxies with $R_i < 3360'' \equiv R_{\mathrm{out}}$, about 1.8 h^{-1} Mpc at a cluster distance of 110 h^{-1} Mpc, where R_i is the projected radial distance of the ith galaxy from the cluster center (R.A. = $16^{\mathrm{h}}03^{\mathrm{m}}11^{\mathrm{s}}$, decl. = 17°55′55″). We have argued that the projected number density $n(R)$ shows a fairly strong falloff toward our maximum R. On the other hand, Figures 5 and 6 show a nonnegligible number of galaxies near the edges of the major axis of the elongation (but not along the minor axis). For the moment, we assume that the projected density of dark matter is proportional to the galaxy $n(R)$, that is, we assume a constant mass-to-light ratio (M/L). Under this assumption there is already some uncertainty introduced by our assigning all galaxies within R_{out} as cluster members and omitting all outside that cutoff. For the variation of M/L introduced below the uncertainty will be much larger.

The dark matter in the cluster is not likely to be associated directly and preferentially with luminous galaxies (see § 6), hence we consider galaxies of any luminosity as equally good tracers of all orbits. We therefore shall use the "number weighted" version of the virial theorem, which defines the total gravitating mass of the cluster as

$$M_{\mathrm{N,VT}} = \frac{3\pi}{2G}\frac{\sum_i v_{zi}^2}{\sum_{ij}(1/R_{ij})}, \tag{2}$$

where $v_{zi} = v_i - v_{\mathrm{av}}$ for the individual galaxies and R_{ij} are the projected separations between galaxy pairs. Using the whole data set yields $V_{\mathrm{av}} = 11{,}059$ km s^{-1} ($\sigma_v = 785$ km s^{-1}), but we shall continue to omit the high-velocity galaxies nos. 13, 26, and 116, so that the remaining 124 galaxies give $V_{\mathrm{av}} = 11043$ km s^{-1}, with $\sigma_v = 715$ km s^{-1}.

Heisler et al. (1985) define the projected mass estimator for extended distribution of mass (such as a cluster),

$$M_{\mathrm{PME}} = \xi\left(\frac{24}{\pi GN}\right)\sum_i v_{zi}^2 R_i, \tag{3}$$

where v_{zi} and R_i are as defined above and ξ is an adjustable constant which depends on the distribution of test particle orbits. They show that, for fully relaxed configurations, $\xi = 2/3$ for radial orbits and $\xi = 4/3$ for isotropic orbits. To facilitate a direct comparison between M_{VT} and M_{PME}, we have used $\xi = 4/3$. We have evaluated both equations (2) and (3) for our 124 galaxies and find

$$\begin{aligned} M_{\mathrm{VT}} &= 4.4 \times 10^{14}\, h^{-1}\, M_\odot, \\ M_{\mathrm{PME}} &= 7.1\xi \times 10^{14}\, h^{-1}\, M_\odot. \end{aligned} \tag{4}$$

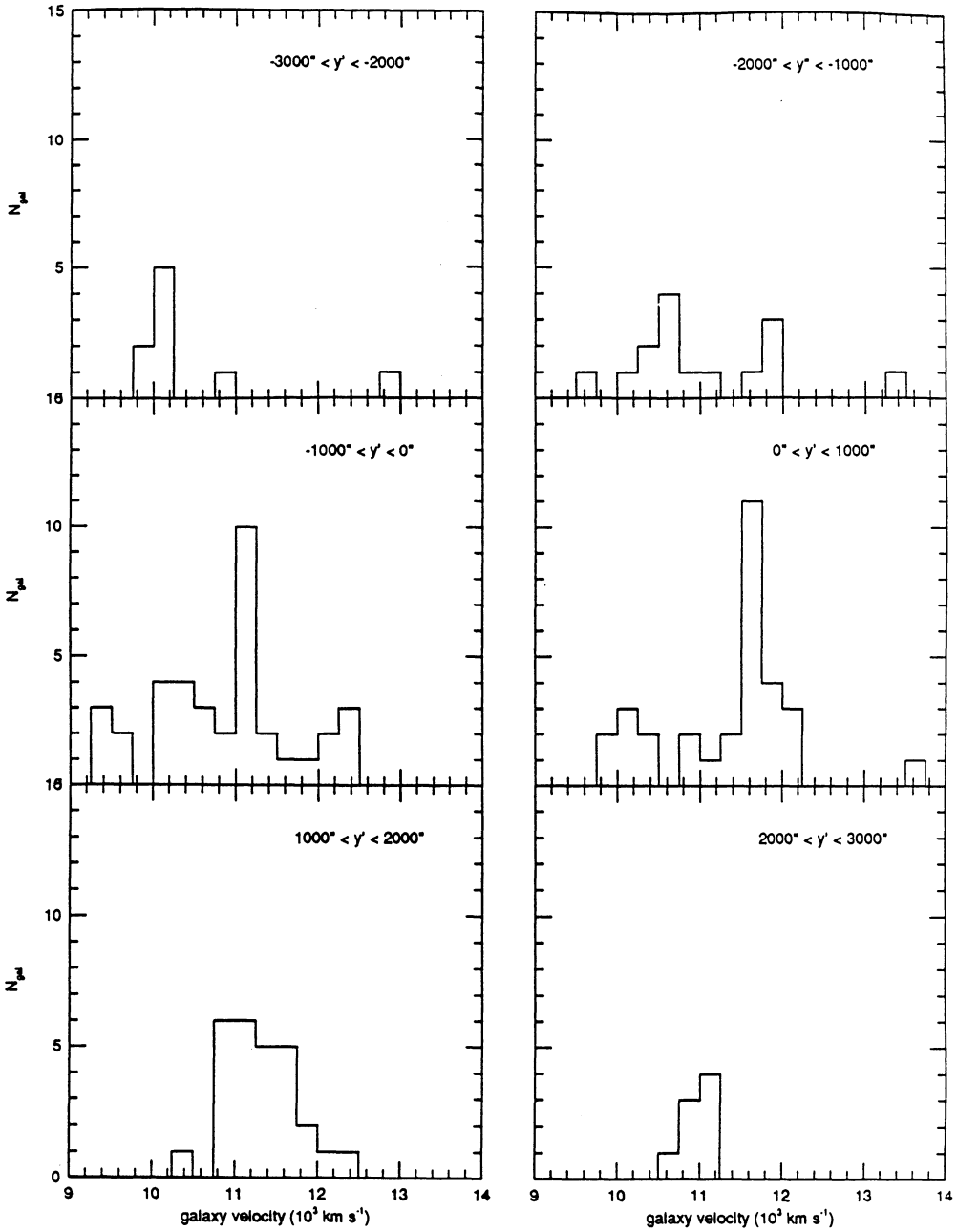

FIG. 7.—Distributions of velocities for galaxies binned along the axis of elongation of A2151 (y' in our nomenclature). Note the particularly small dispersions of the most extreme bins, in the upper left and lower right corners.

The two numerical values in equation (4) are not greatly discrepant, and one might hope that the true value lies somewhere in between, so that the remaining uncertainty would be fairly small. Unfortunately, this is not necessarily the case, and larger systematic errors are possible. We have to distinguish three causes of errors:

1. If there were compact, tightly bound subgroups, much of the gravitational potential energy would come from internal binding. This may lead to an overestimate of the cluster velocity dispersion and therefore an overestimate of the dynamical mass. We have already estimated in the previous section that the presence of substructure introduces a 20% uncertainty in the dynamical mass estimates. To put this another way, although there are indications of the northern clump maintaining its "gravitational integrity," within the overall cluster potential well, this structure does not greatly affect the mass determination (see Bird 1992 for a further discussion of this point).

2. In an otherwise isotropic distribution of orbits, we need also to consider the presence of galaxies which (1) are just now "falling in" with approximately zero total energy orbits and/or (2) have been ejected from the cluster during a "violent relaxation" episode. In both of these cases, V_i^2 tends to be larger than for a relaxed system (by a factor of 2 for the escape speed). In such a case, both values in equation (4) are overesti-

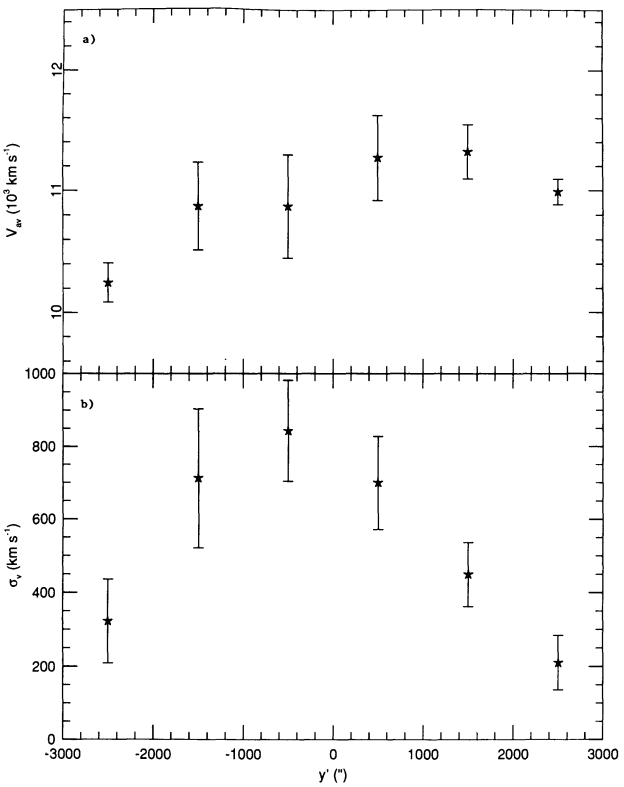

FIG. 8.—Upper panel indicates the average velocity in bins along y' with errors given as the standard deviation about the cluster mean. Lower panel indicates the velocity dispersion itself (as indicated by the deviation about the mean).

mates (the offending orbits are likely to have large R_i and would be weighted more heavily by the projected mass method, which would therefore be the worse overestimate). We have already omitted galaxies nos. 12, 25, and 113 as possible contaminants under these scenarios, and hope that there is little of this kind of effect left. But we cannot exclude the possibility of a true dynamical mass even smaller than M_{VT}.

3. By far the biggest uncertainty is introduced if we allow for a variation in M/L with position in the cluster. Merritt (1987) shows that uncertainties in the underlying distribution in the cluster gravitating matter lead to a range in estimated dynamical masses from 0.4 to 300 times the actual value. One might try to use differences in the velocity dispersion profiles for these different dark matter distributions to constrain these limits more precisely; but in Coma (Merritt 1987; Fitchett & Webster 1987), Hydra I (Fitchett & Merritt 1988), Perseus (Eyles et al. 1991), and other well-studied clusters, as well as here, the measured sets of velocities do not allow discrimination between the predictions of the various models. As the number of velocity measurements for galaxies in clusters increases, and as results from *ROSAT* will allow more precise measurements of mass determined from hot X-ray gas, we may be able to improve our knowledge of the orbital anisotropies in clusters and determine the dark matter distribution more precisely. In any event, as long as circular orbits are more common than radial ones, the mass estimates in equation (4) are better values for the gravitational mass contained in the region where the visible galaxies are concentrated than for the "total cluster mass," that is, the cluster mass to the outer limit of its dark matter distribution, which is entirely unknown to us. For that reason, we have better constraints on the cluster mass-to-light ratio within our R_{max} than we have for the "total cluster mass."

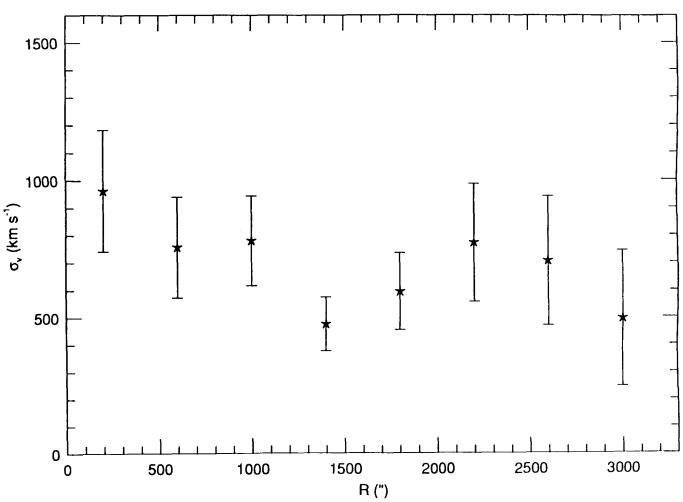

FIG. 9.—The velocity dispersion, as given by the standard deviation about the cluster mean velocity, vs. projected distance from the cluster center.

6. LUMINOSITY AND INDICATIVE MASS

The APS list for Hercules is fairly complete to a limiting magnitude of $m_{ph} = 17.7$. Galaxies of all colors down to this magnitude and out to a radius $2R_c = 3360''$ from the A2151 center yield a photographic luminosity of $1.6 \times 10^{12}\ h^{-1}\ L_\odot$. Adopting $\alpha = -1.25$ and $M*_{ph} = -21.3$ (for $h = 1$) for the Schechter luminosity function (Lugger 1986), we can calculate the multiplying factor F_{Sch} to this observed luminosity to account for light from galaxies below our limiting magnitude. We find $F_{Sch} = 1.2$, and thus $L_{cl} = 2 \times 10^{12}\ h^{-1}\ L_\odot$ for the total cluster luminosity (Tarenghi et al. 1980 had a value about twice as large, due mainly to the use of the Abell luminosity function, which overestimates the contribution from faint galaxies). If we adopt a compromise value of $5 \times 10^{14}\ h^{-1}\ M_\odot$ for the cluster mass, from equation (4), we derive a mass-to-light ratio of $M/L = 250\ h\ M_\odot/L_\odot$. Luminosity here is in the photographic band, which is roughly equivalent to B.

We do not have resolved H I spectra or H I radii R_{HI} for most of our spiral galaxies in A2151, but we have the observed H I velocity widths W_{obs} for the 12 galaxies in Table 1, plus 11 from Giovanelli & Haynes (1985) and 21 from Salpeter & Dickey (1985). For these galaxies, we require an optical diameter from the APS catalog (measured to the 24.1 mag isophote on the blue POSS plate) and an inclination greater than 30° (to minimize uncertainties in the inclination correction to the line widths). These selection criteria leave a total of 20 galaxies in what will be called the 21 cm subset.

For a given galaxy in the 21 cm subset, V_{max} is then given by

$$2V_{max} = W = \frac{W_{obs}}{(1+z)(\sin i)}, \qquad (5)$$

where $z = 0.037$ is the cluster redshift and i is the inclination. We measured the axial ratio b/a for each galaxy from a high-quality optical print of Hercules (kindly provided by A.

Dressler) and used

$$\cos^2(i) = \frac{(b/a)^2 - p^2}{1 - p^2} \quad (6)$$

with $p = c/a = 0.14$, following Haynes & Giovanelli (1984). The "indicative mass" for each spiral galaxy is then given by

$$M_{\rm IND} = 2.33 \times 10^5 V_{\rm max}^2 R_{\rm H\,I}\, h^{-1}\, M_\odot\,, \quad (7)$$

where $V_{\rm max}$, the maximum rotation velocity, is measured in km s^{-1} and $R_{\rm H\,I}$ is taken to be the radius of the neutral hydrogen disk, in kpc. Following Warmels (1986), we assume an average relation of $R_{\rm H\,I} = 1.5R_{25}$ and extrapolate from the 24.1 mags arcsec^{-2} isophotal radius from the APS catalog, after calibrating the optical diameters through comparision with surface photometry of bright ellipticals in Hercules (Strom & Strom 1978; Butcher & Oemler 1985). Data from Giovanelli & Haynes (1985) were used to determine rotational masses for their galaxies in the same fashion. The expression $M_{\rm IND}$ in equation (7) gives the total gravitational mass out to radius $R_{\rm H\,I}$ if one assumes an isothermal mass density distribution, which in turn gives a constant rotation curve.

Table 3 presents the input data and $M_{\rm IND}$ for the 20 galaxies in the 21 cm sample. The sum of these 20 masses is $\sum M_{\rm IND} = 3.3 \times 10^{12}\, h^{-1}\, M_\odot$. The combined luminosity of the 21 cm subset is 11.6% of all those with $m_J < 17.7$ in the APS list. Including the correction $F_{\rm Sch}$ for the fainter galaxies, the ratio of total cluster luminosity to the contribution of the 20 in Table 3 is $f = 10.34$. Assuming the mass-to-light ratio is the same for all galaxies, we then derive for the combined indicative mass

$$M_{\rm IND,\,CORR} = \sum_{\rm radio} M_{\rm IND} \times f = 3.4 \times 10^{13}\, h^{-1}\, M_\odot. \quad (8)$$

The ratio of globally determined cluster mass to the cluster indicative mass is defined as

$$\alpha \equiv \frac{M_{\rm PME}}{M_{\rm IND,\,CORR}} = 20\,. \quad (9)$$

TABLE 3

21 CENTIMETER DATA SET

BDS Catalog Number	Inclination	$V_{\rm max}$ (km s^{-1})	$R_{\rm H\,I}$ (kpc)	$M_{\rm IND}$ ($10^{10}\,M_\odot$)
14	39°	238	12.7	16.8
15	73	157	13.7	7.9
18	73	232	22.3	28.0
20	83	202	11.2	10.6
23	60	187	18.5	15.1
27	84	204	13.7	13.3
36	33	120	8.9	3.0
40	42	234	16.5	21.1
43	70	170	13.7	9.2
50	38	111	20.6	5.9
69	73	139	5.8	2.6
77	79	124	11.4	4.1
93	62	101	12.4	2.9
105	54	315	17.3	40.0
108	76	271	21.6	37.0
112	83	66	10.7	1.1
116	52	233	19.0	24.0
121	66	166	10.9	7.0
122	55	298	12.4	25.7
124	52	244	6.1	8.5

We can see that the parameter α is also a scale length for DM halos in A2151. If these halos are isothermal, then their mass density is proportional to R^{-2}, making $M_{\rm halo}$ proportional to R. Therefore, if the mass in DM exceeds the mass "in" galaxies by α, then $R_{\rm halo}$ exceeds $R_{\rm H\,I}$ by the same amount. Another way to describe the physical significance of α is to point out that $\alpha\ R_{\rm H\,I}$ is the distance to which the galaxian rotation curves must remain flat in order for the galaxies to include all of the globally measured mass. The high number for α indicates that galaxy DM halos must extend to between 150 and 300 kpc for typical spiral galaxy sizes. This is not only appreciably greater than estimates for DM halos in field galaxies (typically 50–100 kpc) (Ashman 1992) but on the order of the intergalaxy spacing in A2151, which implies that the halos must overlap, contradicting the hypothesis that the dark matter is associated with individual galaxies.

7. SUMMARY AND DISCUSSION

The statistical analysis in this paper, which identifies at least one distinct kinematical subunit within the general cluster gravitational potential, supports the view that substructure in clusters is an indication of ongoing dynamical evolution. We have found that substructure in A2151 is significant at a high level, using the diagnostics of Dressler & Shectman (1988b) and West & Bothun (1990). This result is also found in a two-dimensional mixture model analysis of the APS catalog (T. Beers 1992, private communication). The *Einstein* X-ray map of A2151 is bumpy, indicating that the hot intracluster gas, which is presumably a better tracer of the cluster potential than the galaxies, is not smoothly distributed. The fact that the galaxies, their velocities, and the ICM all deviate from smooth isotropic distributions suggests that A2151 is still in the process of collapse. Similarly, its low X-ray flux (Magri et al. 1988) and the lack of hydrogen deficiency in its spirals (Giovanelli & Haynes 1985), along with the high fraction of spirals, are generally interpreted to mean that a cluster is young and relatively unevolved (see also Richstone et al. 1992).

On the other hand, the spiral galaxies do not possess a significantly different spatial distribution or velocity dispersion when compared to the cluster ellipticals. This may mean that unlike the Virgo Cluster, where infalling spirals can be clearly identified (Tully & Shaya 1984), the spirals and ellipticals in Hercules may have existed in the rich cluster environment for similar amounts of time. The α-calculation above suggests that unless cluster galaxies suffer suppression of dark halos during formation in the cluster environment, they have had enough time to interact with the dark matter and each other to undergo some stripping of their dark halos. These are hints that although A2151 is by no means "relaxed," it has already evolved to some extent.

The standard estimators of dynamical mass for A2151 are in the range $3\text{–}9 \times 10^{14}\, h^{-1}\, M_\odot$, but the presence of structure raises further uncertainties. An increase of mass-to-light ratio radially outwards is a possibility which would raise the total mass further, in keeping with arguments by Richstone et al. (1992).

Several further lines of inquiry present themselves. The largest uncertainty in the preceding section is the error in the global mass estimate due to substructure, thus one would like to repeat the α-calculation in a more relaxed cluster. This is problematic for two reasons. As work has proceeded on the structure and dynamics of clusters, it has become apparent that even so-called relaxed clusters, such as Coma and A2256,

possess some anisotropy (Fitchett 1988; Briel et al. 1991). Also, the method requires a high spiral fraction for 21 cm line width measurement, a property which is generally anticorrelated with the degree of dynamical relaxation. At present we are repeating the calculation for the Virgo Cluster, for which we have detailed dynamical mass models and a high number of 21 cm observations, to provide a more accurate measure of α and a direct comparision with a cluster in a different stage of evolution.

Redshift-independent distance measures, such as the Tully-Fisher and the Faber-Jackson relations, may allow a different probe of the distribution of galaxies in A2151. Unfortunately, at the distance of the Hercules Cluster, errors in the Tully-Fisher distances are expected to be comparable to the separation between the galaxies and the subgroups. It is therefore not obvious that these measures are going to allow for a more definite statement about the substructure and distribution of galaxies in this cluster.

Many thanks are owed to Timothy Beers, who provided software, time, and much advice for the adaptive kernel mapping of A2151 and in the use of his robust statistics package, *ROSTAT*. Lyle Hoffman and Alan Dressler graciously provided cluster redshifts and plate material for the verification of the substructure tests. Evan Skillman and Keith Ashman were very helpful in quantifying many of the ideas presented in the final section. This research was supported in part by the National Science Foundation under grant AST 87-22990 to the University of Minnesota and AST 90-15451 to Cornell University.

APPENDIX

ROBUST STATISTICAL ESTIMATORS

The classical estimators of a sample distribution, the mean and the standard deviation, efficiently reproduce the properties of the underlying parent distribution only when that underlying distribution is a pure Gaussian. In situations where contamination of the data set is suspected, these estimators are highly susceptible to confusion. For instance, a Gaussian which is contaminated by a few data points in the tails will consistently yield a standard deviation which is spuriously high.

In the past, the assumption has been that velocity distributions in clusters of galaxies are isotropic and Gaussian (see, e.g., Yahil & Vidal 1977), and therefore that the sample mean and standard deviation are the most appropriate measures of the average velocity

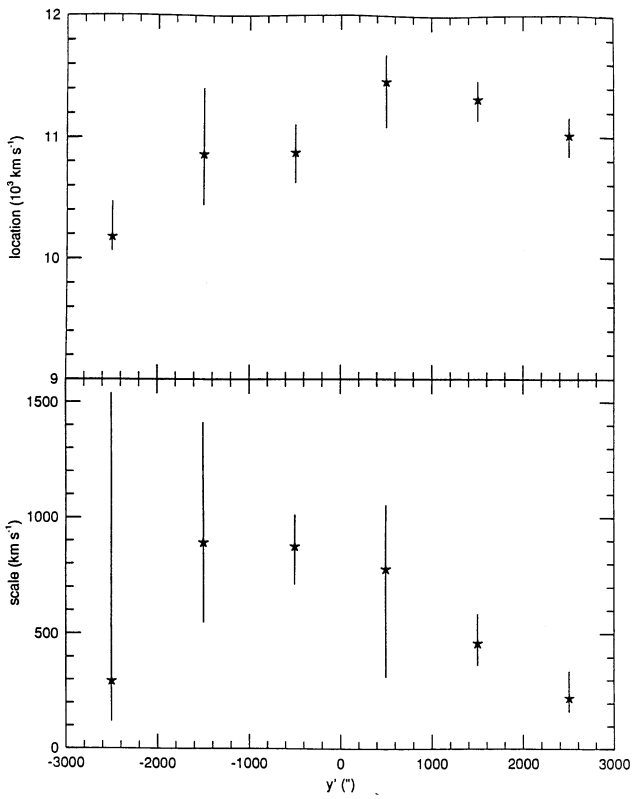

FIG. 10

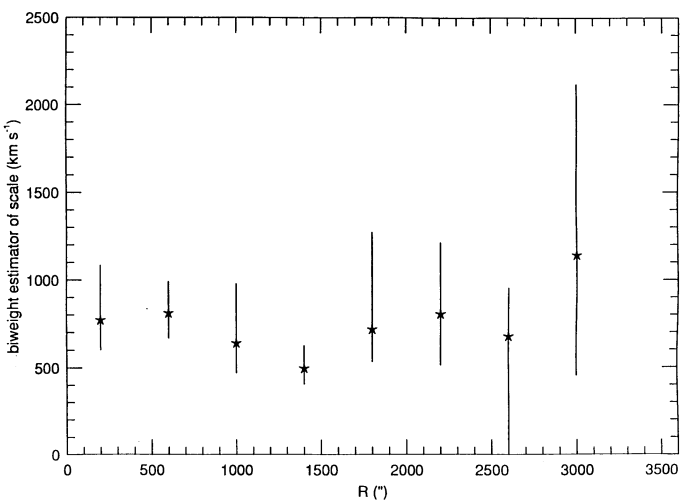

FIG. 11

FIG. 10.—The biweight estimators of velocity location, C_{BI} (*upper panel*), and scale, S_{BI} (*lower panel*), for 1000″ bins along the y' axis. This is the statistically robust version of Fig. 8 (see Beers et al. 1990 for a complete description of these estimators and their associated errors).

FIG. 11.—The biweight estimator of scale—the statistically robust determination of the velocity dispersion—vs. projected radius within A2151. Error bars are the bootstrap estimates of the confidence intervals about these values.

and velocity dispersion. We currently have much reason to believe that these assumptions are dangerous: this work, along with many others, shows the likelihood of small-scale velocity anisotropy among clusters of galaxies, both from kinematic and positional data (see references herein) and from X-rays (Eyles et al. 1991; Briel et al. 1991). For this reason, the sample mean and the standard deviation are suspect estimators of the characteristics of the parent population. In the common situation where the nature of the underlying population and contamination is unknown, Beers et al. (1990) recommend the biweight estimators of location C_{BI} (a robust analog of C_μ, the sample mean) and scale S_{BI} (the robust version of S_σ, the standard deviation) as the most efficient and resistant estimators of the properties of the data set.

We have used the FORTRAN code *ROSTAT*, kindly provided by Timothy Beers, to calculate the location and scale for the complete A2151 data set. Figure 10 is the robust version of Figure 8 of the main text: the upper panel is the velocity location C_{BI} versus y', the major axis of elongation, in the cluster. Here, the error bars are the confidence intervals determined by bootstrapping the original data set. The lower panel is the velocity scale S_{BI} versus y', with similarly calculated confidence intervals. Here, although the confidence intervals are large, we see that the scale of the data set drops significantly (by about 50%) in the most distant y' bins, $-3000'' < y' < -2000''$ and $2000'' < y' < 3000''$. This strongly supports the argument for the physical integrity of the northern subgroup identified by the Dressler-Shectman test. A similar plot along the x'-axis yield no drop in the area of the third clump hinted at in text Figure 5, but there were only five galaxies in the appropriate x' bin and so the results are not yet clear.

Figure 11 is the robust version of text Figure 9, S_{BI} versus projected radius R within the cluster, with bootstrapped confidence intervals. This is discussed briefly in § 5.

ROSTAT also provides statistical measures of a data set's deviation from normality. Despite the irregular shape of the general cluster velocity histogram, these tests, including the measures identified by Yahil & Vidal (1977) as well as others, do not indicate a statistically significant deviation. The tail index described by Beers et al. (1991) does show that the distribution is light-tailed compared to Gaussian, as we expect from the boxy appearance of the histogram. This hints at the unresolved structure in the velocity distribution which we discuss in § 4.

Finally, we have calculated a robust estimator of the virial mass, following Beers et al. (1991). This value is $M'_{VT} = 4.5 \times 10^{14}\ h\ M_\odot$ for $C_{BI} = 11{,}084\ \mathrm{km\ s^{-1}}$ and $S_{BI} = 731\ \mathrm{km\ s^{-1}}$, which is essentially identical with the standard virial theorem estimate.

For more detail on these methods, see Beers et al. (1990), from which we have borrowed heavily.

REFERENCES

Ashman, K. M. 1992, PASP, in press
Bahcall, J. N., & Tremaine, S. 1981, ApJ, 244, 805
Beers, T. C., Flynn, K., & Gerbhardt, K. 1990, AJ, 100, 32
Beers, T. C., Forman, W., Huchra, J. P., Jones, C., & Gebhardt, K. 1991, AJ, 102, 1581
Beers, T. C., & Tonry, J. L. 1986, ApJ, 300, 557
Begeman, K. 1987, Ph.D. thesis, Univ. Gronigen
Bicay, M., & Giovanelli, R. 1986, AJ, 91, 705
Binney, J., & Tremaine, S. 1987, Galactic Dynamics (Princeton: Princeton Univ. Press)
Bird, C. M. 1992, master's thesis, Univ. Minnesota
Bothun, G. D., Geller, M., Beers, T. C., & Huchra, J. 1983, ApJ, 268, 47
Bridle, A. H., Davis, M. M., Fomalont, E. B., & Lequeux, J. 1972, AJ, 77, 405
Briel, U. G., Henry, J. P., Schwarz, R. A., Bohringer, H., Ebeling, H., Edge, A. C., Hartner, G. D., Schindler, S., Trumper, J., & Voges, W. 1991, A&A, 246, L10
Buote, D. A., & Canizares, C. R. 1992, preprint, MIT No. CSR-92-11
Butcher, H., & Oemler, A., Jr. 1985, ApJS, 57, 665
Casertano, S., & van Gorkam, J. 1991, AJ, 102, 1231
Dickey, J. M., Keller, D. T., Pennington, R., & Salpeter, E. E. 1987, AJ, 93, 788
Dressler, A., & Shectman, S. 1988a, AJ, 95, 284
———. 1988b, AJ, 95, 985 (DS)
Eyles, C. J., Watt, M. P., Bertram, D., Church, M. J., Ponman, T. J., Skinner, G. K., & Willmore, A. P. 1991, ApJ, 376, 23
Faber, S. M., & Gallagher, J. S. 1979, ARA&A, 17, 135
Fitchett, M. J. 1988, in The Minnesota Lectures on Clusters of Galaxies and Large Scale Structure, ed. J. M. Dickey (San Francisco: Astronomical Society of the Pacific), 143
Fitchett, M. J., & Merritt, D. 1988, ApJ, 335, 18
Fitchett, M. J., & Webster, R. 1987, ApJ, 317, 653
Freudling, W. 1990, Ph.D. thesis, Cornell Univ.
Freudling, W., Haynes, M., & Giovanelli, R. 1992, ApJS, in press
Geller, M., & Beers, T. C. 1982, PASP, 94, 421
Giovanelli, R., Chincarini, G. L., & Haynes, M. 1981, ApJ, 247, 383
Giovanelli, R., & Haynes, M. 1985, ApJ, 292, 404
Grossman, S. A., & Narayan, R. 1989, ApJ, 344, 637
Haynes, M., & Giovanelli, R. 1984, AJ, 89, 758
Heisler, J., Tremaine, S., & Bahcall, J. 1985, ApJ, 298, 8 (HTB)
Hoffman, G. L., Helou, G., Salpeter, E. E., & Lewis, B. M. 1989, ApJ, 339, 812
Hoffman, G. L., & Salpeter, E. E. 1982, ApJ, 263, 485
Huchra, J. P. 1990, preprint (the Redshift Catalog)
Kent, S. M., & Gunn, J. E. 1982, AJ, 87, 697
Lucey, J. R., Currie, M. J., & Dickens, R. S. 1986, MNRAS, 221, 453
Lugger, P. M. 1986, ApJ, 303, 535
Magri, C., Haynes, M., Forman, W., Jones, C., & Giovanelli, R. 1988, ApJ, 333, 136
Merritt, D. 1985, ApJ, 289, 18
———. 1987, ApJ, 313, 121
Puche, D. 1991, Ph.D. thesis, Univ. Montreal
Richstone, D., Loeb, A., & Turner, E. L. 1992, preprint
Salpeter, E. E., & Dickey, J. M. 1985, ApJ, 292, 426
Schommer, R. A., Sullivan, W. T., & Bothun, G. D. 1981, AJ, 86, 943
Strom, K. M., & Strom, S. E. 1978, AJ, 83, 1293
Tarenghi, M., Chincarini, G., Rood, H. J., & Thompson, L. A. 1980, 235, 724
Tarenghi, M., Tifft, W. G., Chincarini, G., Rood, H. J., & Thompson, L. A. 1979, ApJ, 234, 793
Tully, R. B., & Shaya, E. J. 1984, ApJ, 281, 31
Tyson, J. A. 1992, Phys. Today, 45, 24
Warmels, R. H. 1986, Ph.D. thesis, Univ. Groningen
West, M. J. 1990, in Clusters of Galaxies, ed. W. R. Oegerle, M. J. Fitchett, & L. Danly (New York: Cambridge Univ. Press), 65
West, M. J., & Bothun, G. D. 1990, ApJ, 350, 36
Yahil, A., & Vidal, N. V. 1977, ApJ, 214, 347